Available online at www.sciencedirect.com

ScienceDirect

Procedia Computer Science 126 (2018) 723–732

Procedia Computer Science

www.elsevier.com/locate/procedia

International Conference on Knowledge Based and Intelligent Information and Engineering Systems, KES2018, 3-5 September 2018, Belgrade, Serbia

A robust anisotropic edge detection method for carotid ultrasound image processing

José Rouco[e,f], Catarina Carvalho[a], Ana Domingues[a], Elsa Azevedo[c,d], Aurélio Campilho[a,b]

[a] *INESC TEC - INESC Technology and Science, FEUP, Porto, Portugal*
[b] *FEUP - Faculty of Engineering, University of Porto, Rua Dr. Roberto Frias s/n, Porto 4200-465, Portugal*
[c] *FMUP - Department of Clinical Neurosciences and Mental Health, Faculty of Medicine, University of Porto, Porto 4200-319, Portugal*
[d] *Department of Neurology, São João Hospital Center, Porto 4200-319, Portugal*
[e] *CITIC - Research Center of Information and Communication Technologies, UDC, A Coruña, Spain*
[f] *Department of Computer Science, University of A Coruña, Campus de Elviña s/n, A Coruña 15071, Spain*

Abstract

A new approach for robust edge detection on B-mode ultrasound images of the carotid artery is proposed in this paper. The proposed method uses anisotropic Gaussian derivative filters along with non-maximum suppression over the overall artery wall orientation in local regions. The anisotropic filters allow using a wider integration scale along the edges while preserving the edge location precision. They also perform edge continuation, resulting in the connection of isolated edge points along linear segments, which is a valuable feature for the segmentation of the artery wall layers. However, this usually results in false edges being detected near convex contours and isolated points. The use of non-maximum suppression over pooled local orientations is proposed to solve this issue. Experimental results are provided to demonstrate that the proposed edge detector outperforms other common methods in the detection of the lumen-intima and media-adventia layer interfaces of the carotid vessel walls. Additionally, the resulting edges are more continuous and precisely located.

Keywords: edge detection; anisotropic filter; carotid ultrasound; intima-media;

1. Introduction

Atherosclerosis is a vascular disease characterized by the thickening of the artery wall and the formation of atheromatous plaques. It constitutes the main pathological mechanism underlying stroke and myocardial infarction, which are the leading causes of death and permanent disability in developed countries. The early diagnosis of the disease is very important in order to reduce the morbidity and disability rates [1]. B-mode ultrasonography of the arteries, such as the extra-cranial portion of the carotid, has become widely used in clinical practice for the diagnosis of atherosclerosis and associated diseases, as it is a high-resolution, non-invasive, low cost and readily available medical imaging

E-mail address: jrouco@udc.es, campilho@fe.up.pt

1877-0509
10.1016/j.procs.2018.08.006

technology. These images allow the visualization of the anatomical layers of the vessel walls, so that from a longitudinal B-mode ultrasound image of the common carotid artery (CCA) it is possible to measure the thickness of the intima-media complex, the lumen diameter, or the identification, measurement and assessment of atherosclerotic plaques[2,3]. The distance between the inner boundary of the adventitia and the lumen, the so-called intima-media thicknes (IMT), is being increasingly used as a surrogate marker of atherosclerosis in several clinical studies which have demonstrated the ability to predict future risk of clinical vascular events[4,5,6,7]. These measurements are obtained in plaque-free regions, where the intima-media complex is flat, and its boundaries are parallel straight lines. Plaque related measurements also require the segmentation of the intima-media complex, but in areas where the thickening is larger than usual. The plaque regions usually require more complex segmentation algorithms, as their shape and inner characteristics have a large variability that are not easily modeled with straight parallel lines.

In early approaches for marker measurement, the segmentation is often performed manually by clinical experts, with the disadvantage of being a time-consuming process that limits the amount of exams and the number of observed patients. Manual segmentation is also subjective, resulting in large intra- and inter-observer marker variability[8]. There is a growing interest in automatic and semi-automatic segmentation methods that increase the accuracy and reproducibility of the measures and reduce the subjectivity and time of analysis by minimizing the user interaction requirements. The automatic measurement of IMT has received much attention during the last few years, with some works achieving enough intima-media measurement precision for clinical practice use[9,8]. Most of the methods are focused in the segmentation and measurement of a plaque-free region where a double-line pattern, corresponding to the lumen-intima and media-adventitia layer transitions, is clearly visible[2]. This allows the use of straight segments and parallelism as shape priors for the segmentation[10,11], but usually demanding user definition of the measurement region of interest (ROI). There are also a few methods aiming for the automatic segmentation of plaque regions, that usually require user interaction for ROI selection and intensity normalization[12,13,14,8]. Finally, some other methods consider the segmentation of the whole extent of the intima-media complex, including the plaque and plaque-free regions[15,16]. Regardless of the method used for ROI selection and the definition of the contours contributing to the segmented regions, image processing stages that allow a robust edge detection, dealing with the inherent complexity of ultrasound images, are necessary. This work is focused in this aspect.

Ultrasound images are characterized by the presence of speckle noise and local changes of intensity and contrast. The echogenicity of the CCA lumen and walls do not only depends on their tissue composition, but also depends on the insonation angle, the tissue attenuation, and on the ultrasound gain parameter settings. Although the acquisition protocols for ultrasound-based measurement aim at standardizing the overall aspect of the CCA images[2,3], these ultrasound settings are ultimately established according to the subjective judgment of the operator. Thus, the acquisition procedures are completely manual, and a high skill is required to achieve good and useful images. Even more, it may not be possible to achieve homogeneous imaging of the artery walls along the whole width of the image. This complicates the proposal of fully automated methods, and affects the required robustness of the edge detection methods, as contrast and intensity vary along the image, and several non-relevant edges appear in the homogeneous tissue regions. For these reasons, it is required that the edge detectors use some additional assumptions to separate true and false edges.

1.1. Related work

Regarding CCA segmentation, this work builds upon the automatic approaches proposed in[15] and[16]. These methods, as with the CCA detection methods in[17,18], use a dynamic programming (DP) optimization approach to trace the boundaries of the intima-media region, traversing from one side of the image to the other. These two methods first compute the image edges as local maxima of the instantaneous coefficient of variation (ICOV) as proposed in[19,20]. Then, the detected edge points are filtered according to several heuristics to create suitable edge maps for each of the target boundaries, which are then used as a gain map in the DP process.

ICOV is well suited for ultrasound images because it is derived from speckle denoising methods[19]. In this sense, it is assumed that the image regions follow a multiplicative noise model that can be estimated from the local information, and removed from the original image data. However, the speckle filtering capabilities of the ICOV are best suited when applied in an anisotropic diffusion scheme[20], so that the effective filter scale, in which the statistics are estimated, is higher in flat areas and smaller near edges, avoiding the image smoothing near the edges. While this approach can avoid the detection of edges in noisy flat areas, it does not enhance the detection of subtle boundary edges between

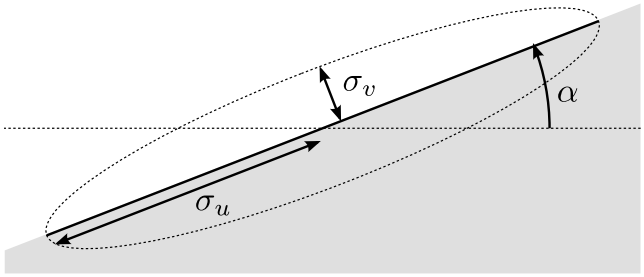

Fig. 1: Example of oriented anisotropic Gaussian filter

low contrast tissues. Thus, some edge points in these boundaries may be filtered, resulting in less continuous edge features. Additionally, the diffusion is driven by the ICOV itself, and the amount of diffusion applied, which is hard to control, affects the trade-off between the preserved edges and the denoised regions.

In this work, instead, we propose the use of a bank of anisotropic Gaussian derivatives for edge detection. The assumption underlying this proposal is that interesting boundaries are highly linear, and thus the contrast changes are preserved in a local region of nearby pixels. With this approach we aim at the opposite effect of the ICOV, trying to enhance edge features that follow a coherent behavior along a low curvature continuous boundary, even at low contrast, assuming the risk of eventually enhancing some of the noise in flat areas. Thus, the probability of finding a continuous edge path along low contrast boundaries, like the lumen-intima tissue interface, is higher, along with the probability of finding a wrong path through image artifacts and noise. The detection of candidate continuous boundaries is of much higher recall and slightly lower precision, which is more suitable for semi-automatic methodologies, that relies on the user for the final selection of the correct boundary, but the dynamic programming-based automatic approaches may also take advantage of these features.

2. Robust anisotropic edge detection

We propose the use of highly anisotropic Gaussian derivatives for edge detection in B-mode ultrasound images of the carotid. The usual issue with edge detection in ultrasound images is the presence of speckle noise, which is a multiplicative noise that gives rise to grainy textures. In this type of images, the small scale finite difference filters, like Sobel filters, result in a high number of edge points due to the noise. An usual solution on noisy edge pixels is the use of Gaussian derivative filters, so that the finite differences are computed on low-pass Gaussian filtered images with a large enough σ, and the noisy edges are filtered out. However, Gaussian filters are not specifically well-suited for removing multiplicative noise in homogeneous tissue areas. Also, increasing the scale parameter σ causes accuracy and precision loss in the estimated edge locations, as well as the smoothing of corner shapes and blending of nearby edges. This is specially relevant in intima-media region segmentation applications, where the segmented contours are used for measurement.

Thus, the use of large scale filters for edge detection is interesting to reduce the effect of the noise, while small scales are better for accurate and precise estimation of the edge locations. For this reason, we propose to use oriented anisotropic Gaussian derivatives, with a larger scale in the edge boundary direction, and a smaller scale in the perpendicular analysis direction, along which the derivative is computed. An example of this is depicted in Fig. 1. The idea is to allow the filter to integrate local image information to provide a more robust, precise and accurate edge detection. However, it is required that the target boundaries are locally linear. Even though, this is the case in intima-media segmentation, as the target boundaries have low curvature in comparison with the pixel size, while it is usually required an edge precision and accuracy in the order of the pixel size. Thus, we can design these filters with a large scale compatible with the intima-media region anatomy, while preserving the small analysis scale in the order of the image pixel size.

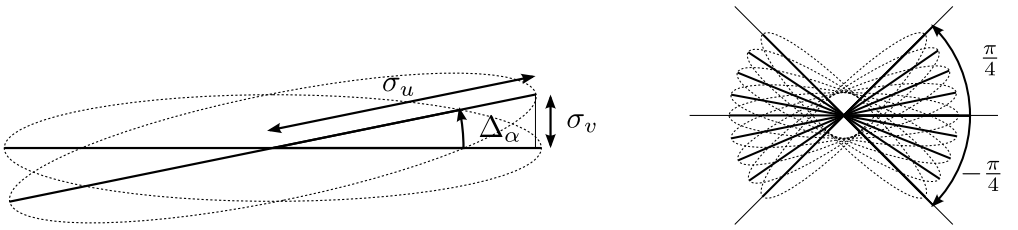

(a) (b)

Fig. 2: Computation of Δ_α based on filter overlap. a) Graphical example. b) Resulting filter bank.

2.1. Anisotropic Gaussian derivative filter bank

The oriented Gaussian filter g_α, and the oriented Gaussian derivative filter g'_α, in the α direction are given by

$$g_\alpha = g(x, y; \sigma_u, \sigma_v, \alpha) = \frac{1}{2\pi\sigma_u\sigma_v} \exp\left(-\frac{u_\alpha^2}{2\sigma_u^2} - \frac{v_\alpha^2}{2\sigma_v^2}\right) \tag{1}$$

$$g'_\alpha = \frac{\partial}{\partial v_\alpha} g_\alpha \tag{2}$$

where σ_u controls the scale along the α direction and σ_v controls the scale along its perpendicular. The transformed coordinates in the α direction and its perpendicular, that are denoted as $u_\alpha = u(x, y; \alpha)$ and $v_\alpha = v(x, y; \alpha)$ respectively, are derived from

$$\begin{pmatrix} u_\alpha \\ v_\alpha \end{pmatrix} = \begin{pmatrix} \cos\alpha & \sin\alpha \\ -\sin\alpha & \cos\alpha \end{pmatrix} \begin{pmatrix} x \\ y \end{pmatrix} \tag{3}$$

The oriented Gaussian derivative filter g'_α is well suited for detecting edges in the α direction. In order to cover the whole range of orientations of the intima-media boundaries we create a bank of filters G' as

$$G' := \{\, g'_\alpha \mid \alpha = k\Delta_\alpha, k = -N, \ldots, N\} \tag{4}$$

where the orientation increment Δ_α is computed to ensure a good filter overlap at the longitudinal extremes as

$$\Delta_\alpha = \arcsin \frac{\sigma_v}{\sigma_u} \tag{5}$$

where σ_u and σ_v are the filter scales used in equation (1). Fig. 2(a) depicts a graphical example of the orientation increment based on the filter overlap. The $2N + 1$ filters in the bank cover orientations from at least $-\pi/4$ to $\pi/4$ as depicted in Fig. 2(b). This is achieved computing N as

$$N = \left\lceil \frac{\pi}{4\Delta_\alpha} \right\rceil \tag{6}$$

Using the filter bank G' we compute each of the anisotropic oriented Gaussian derivative responses I'_α, for the target image I, by convolving each filter $g'_\alpha \in G'$ with the image, and we denote the set of $2N + 1$ responses as I'.

Edge detection can be performed using oriented non-maximum suppression on each channel. In order to detect local maxima and minima, we compare the $I'_\alpha(x, y)$ values with their nearby positions $I'_\alpha(x \pm \delta \sin\alpha, y \pm \delta \cos\alpha)$ in the direction of analysis of the filter, at an offset distance of δ pixels.

Likewise, channel combination can be performed by taking the filter value at the orientation with the highest absolute derivative value at each point. This can be used to either combine gradient or edge channels by taking the orientation that is the best fit for the pixel neighborhood, according the filter response. However, this orientation estimation is sensible to noise. The anisotropic filters give slight local maxima responses at background positions in

the direction of the nearby edges. This implies that speckle points, line-ends, or any other strong edges in the image may result in locally high filter responses for all the orientations in a neighborhood of size σ_u around them, which may result in star-like edge responses.

In order to avoid this issue, we propose to make a more robust orientation estimation for channel combination and pooling. The idea is to perform a pooling of responses in a large neighborhood around each point to detect the most dominant orientation in that region. We thus compute the dominant local orientation $\tilde{\alpha}(x, y)$ for each point following the equation

$$\tilde{\alpha}(x, y) = \arg\max_{\alpha} \left[g_\beta * \exp\left(\left|I'_\alpha\right|\right)\right](x, y) \tag{7}$$

where g_β is an oriented anisotropic Gaussian filter, as defined in equation (1), with $\beta = \alpha + \pi/2$ in the perpendicular orientation to each filter channel, and $|\cdot|$ denotes the absolute value. The Gaussian average of the exponential absolute response results in a *softmax* effect, accounting for the highest edge responses with α orientation for all the positions at distance below σ_u in the perpendicular direction. The pooled response will be higher for orientations with one or several parallel strong edges, than for orientations with many small edge values. The maximum over the orientation will then prefer the orientations with fewer strong edges. Note that in equation (7) the edge sign is not taken into account and both edge directions vote for the dominant local orientation. This is useful for the case of longitudinal B-mode images of the carotid, as the artery walls are usually composed of several parallel layers, which allow for a very robust wall orientation estimation. In this way, the proposed method allows to only detect and take into account the edges following a coherent wall direction for which the edge strengths are significantly higher than the granular texture around them, while preserving the edge location precision and accuracy.

The σ_u and σ_v of the Gaussian filter used for pooling can be different from those used for the derivatives. Equal values usually make sense for σ_v, as it depends on the image resolution and required precision for the edge detector, while the σ_u would depend on the anatomic features of the target boundaries. In this work we use σ_v equal to $1/2\,px$, while σ_u is in the order $1\,mm$ for the Gaussian derivatives, which is slightly higher than a regular IMT (about $0.8\,mm$). We use half this value for the pooling, allowing to ensure that the target intima-media and media-adventitia boundaries fall into separate pooling regions. These parameters result in a bank of 37 filters for images with $0.09\,mm/px$ resolution. However, a higher σ_v is probably valid for images with a higher resolution, allowing to keep the required number of filters for larger images. Each one of these filters requires an initial convolution with the image for computing the derivatives, plus and additional convolution for the pooling. Thus, in order to keep the computation time in the interactive range, it is necessary to use an efficient method for the computation of anisotropic oriented Gaussian filters. We achieve this using the implementation proposed in [21], reducing the computation time of the filter responses to few seconds in a modern workstation.

3. Experimentation and results

3.1. Image dataset

An image dataset of 200 B-mode images of the CCA, acquired with an ATL-HDI5000 ultrasound system, is used for the experiments. This dataset is the same as the one used in [18], and consists of 50 images from Hospital São João in Porto (Portugal), plus 150 additional images provided by Dr. Filipo Molinari, from Universty of Torino (Italy). The pixel size of all the images is normalized to 0.09 mm using linear interpolation resampling, to ease the setting of scale-dependent parameters in the algorithms. Four manual contours are associated to each image, corresponding to the media-adventia (MA) and lumen-intima (LI) tissue interfaces for both the far-wall (FW) and near-wall (NW) intima-media regions, that are used as ground truth (GT) for the edge detector. These manual delineations do not cover the whole extent of the image horizontally, thus only the image columns with existent ground truth are considered in the experiments for each contour.

3.2. Edge detection methods in the comparison

The gradients at the NW boundaries point down, while they point up for the FW. In order to account for the gradient direction the sign of the filter bank responses is considered in the non-maximum suppression process, and opposite signs are used to detect the NW and FW boundaries.

The proposed edge detector combines the anisotropic Gaussian derivative filters and the proposed non-maximum suppression using the local pooling orientation estimation. This approach is denoted in the experiments as "Anisotropic local". It is compared with the straightforward combination of the filter responses by preserving the orientation with highest response, which is denoted as "Anisotropic".

Two additional edge detectors are considered for comparison. The first one, denoted as "Isotropic", consists on regular non-maximum suppression over isotropic Gaussian derivatives with scale $\sigma = \sigma_v$. This is the most commonly used method for edge detection. The last method consist on the "ICOV" edge detector, using Gaussian derivatives of scale $\sigma = \sigma_v$. This edge detector is included in the comparison because it has been used before for intima-media segmentation in [15] and [16].

3.3. Evaluation metrics

Receiver Operating Characteristic (ROC) and precision-recall (PR) curves are used to evaluate the performance of the proposed edge detectors. However, we do not consider all the image pixels for the evaluation of each target contour, as the results would be misled the presence of the other target contours and relevant contours corresponding to other anatomical structures. Instead, only a small region of interest around each contour, in which the target contour should be unique, is considered. This region is delimited by each of the GT contours displaced by a fixed distance $0.5\,mm$ up and down ($6\,px$ for these images). This distance is lower than the minimum, and higher than half of the average, regular IMT for a healthy individual [18], which guarantees that the region only contains edges of the LI or the MA for each wall. On the other hand, the GT contours may not be precisely located over the actual best edge pixels. For this reason, we consider a tolerance distance τ, below which detected edges are considered as true positives (TP). However, care should be taken to only assign one edge pixel as TP for each GT position. For this reason, only the closest edge point for each column is counted as TP, while the rest of detected edge points are added to the false positives. This approach is similar to the one used in [22].

Both the area under the ROC and the PR curves (*AUC-ROC* and *AUC-PR*) are considered, as they allow to evaluate the edge detectors independently of the used threshold. However, we consider that the *AUC-PR* statistic is more representative of edge detection performance, as false negatives are less relevant than false positives. We consider two different approaches for AUC computation: global and image-wise. In the global approach the same threshold is applied to all the images to compute the confusion matrix, and the *AUC-ROC* and the *AUC-PR* values are computed for the whole dataset. In image-wise approach, instead, the *AUC-ROC* and *AUC-PR* are computed for each of the image separately, and both the average and standard deviation are reported. This latter approach allows to evaluate the edge detector when the optimal threshold is used for each image, and provides an estimation of the performance variability. Two additional statistics are evaluated to assess the quality of the detected contours. First, the average distance between the TP and the GT ($d(TP)$) is computed for each threshold in the ROC and PR curves. This allows to assess and compare the precision of the detected contours regardless of the used tolerance threshold τ. The second statistic consists on the average number of connected TP components, normalized by the number of TP (CC/TP). This allows to evaluate the continuity of the resulting edges. Continuous edge segments are usually preferred for posterior analyses, and specially well-suited for dynamic programming based segmentation methods [15,16]. Global and image-wise approaches are also considered for the computation of these statistics.

3.4. Results and discussion

An example of the resulting edges in two regions around the NW and FW are shown in Fig. 3. The edge maps are depicted without applying any threshold. The GT contours are also depicted in dotted lines. It is observed that the proposed method provides the cleanest edge maps. Fig. 4 depicts the evolution of the global *AUC-PR* with varying tolerance τ for all the four target contours. It is observed that the relative comparison of methods does not change with the varying detection tolerance. Note, however, that a tolerance of at least $\tau = 3\,px$ is necessary to stabilize the results. The best results, as expected, are obtained for the MA contours, with the methods showing a similar behavior for both the near and far walls. The proposed method achieves the highest *AUC-PR* among all methods. The second best method is the highest response anisotropic approach, without the use of local orientation estimation. Both the ICOV and the regular Gaussian derivative filters achieve a similar result. In the case of the LI contours, again, a similar result is obtained for both walls. For these contours, the proposed anisotropic method provides a higher improvement with

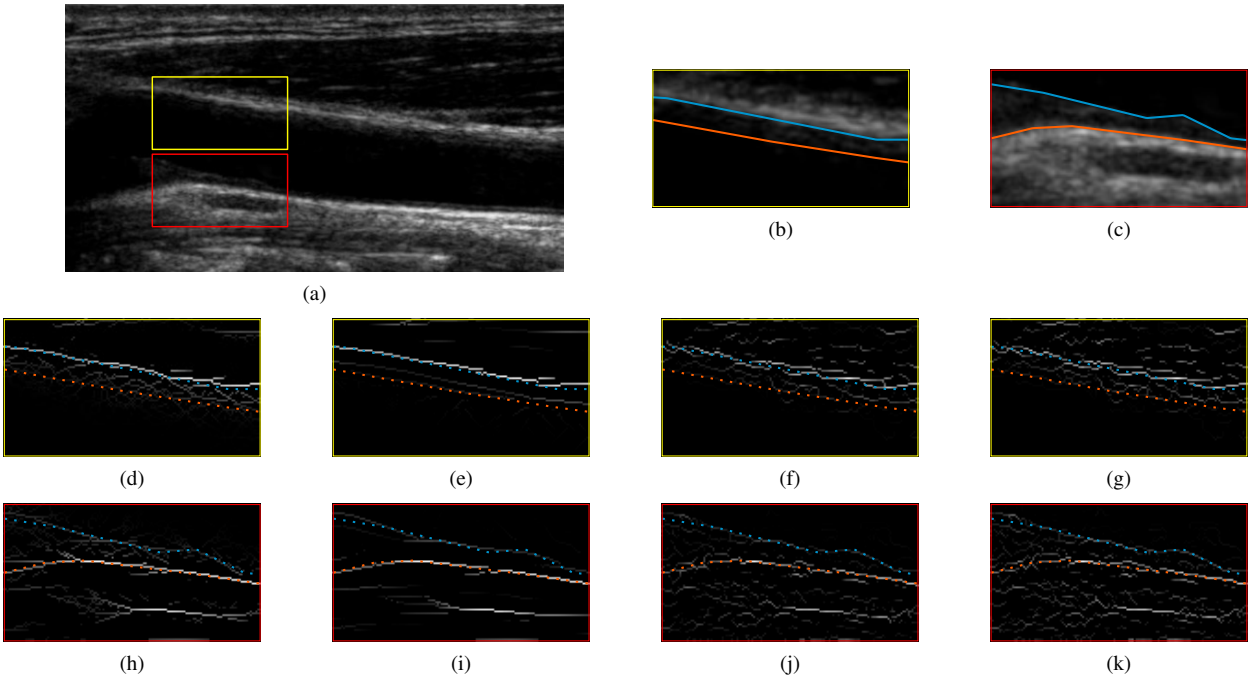

Fig. 3: Example edge maps using the compared methods. a) Original image with zoom regions depicted for NW and FW. b) Zoom region for NW. c) Zoom region for FW. d-g) NW results using the anisotropic (d), anisotropic local (e), isotropic (f) and ICOV (g) methods. h-k) FW results using the anisotropic (h), anisotropic local (i), isotropic (j) and ICOV (k) methods.

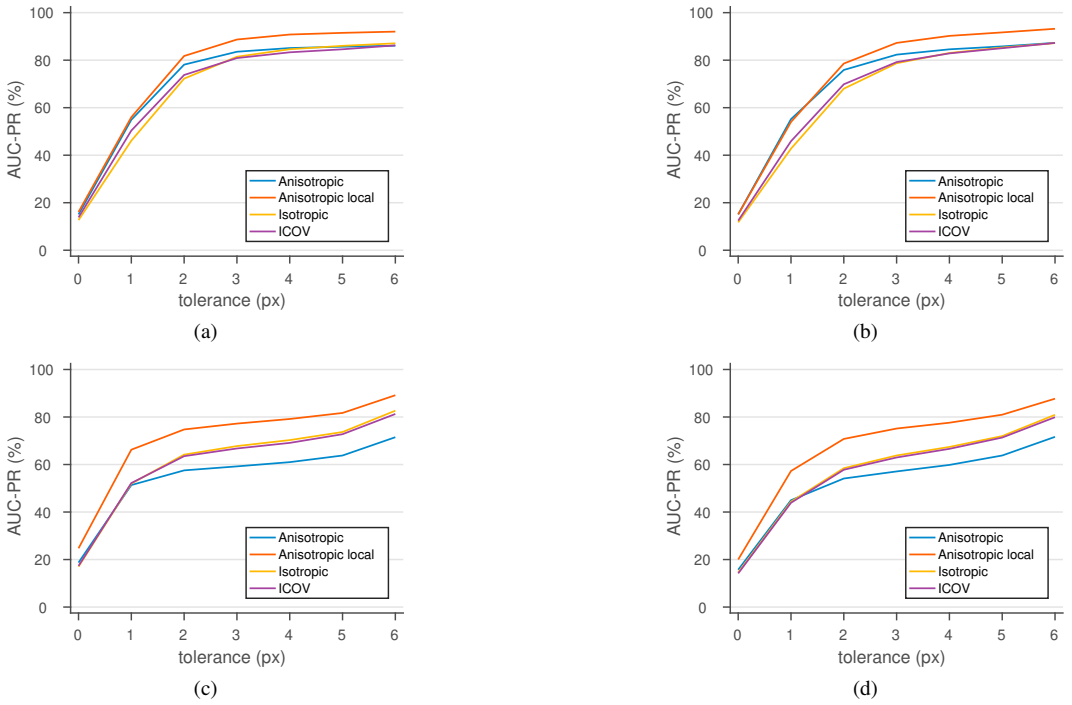

Fig. 4: Area under precision-recall curves with varying tolerance τ values for the different target contours. (a) Far-wall media-adventitia. (b) Near-wall media-adventitia. (c) Far-wall lumen-intima. (d) Near-wall lumen-intima. The results show that the proposed anisotropic edge detector, using the non-maximum suppression over local orientation, achieves a higher *AUC-PR*, regardless of the tolerance parameter used for the evaluation.

Table 1: Comparison results measured for tolerance $\tau = 3$. *AUC-ROC* and *AUC-PR* denote the percentage of area under the ROC and precision-recall curves, respectively. CC/TP denote the percentage of connected components per true positive at 90% recall. $d(TP)$ is the average distance between the true positives and the ground truth at 90% recall. The statistics are computed using the global and the image-wise approaches described in section 3.3. The results indicate that the proposed anisotropic edge detector, using the non-maximum suppression over the local orientation, allows to detect higher quality contours with higher precision, regardless of the evaluated intima-media contour.

		AUC-ROC (%)		*AUC-PR* (%)		CC/TP (%)		$d(TP)$ (px)	
FW-MA	Anisotropic	97.88	**98.64 ± 1.76**	83.55	88.92 ± 11.86	8.77	4.08 ± 3.51	2.00	1.55 ± 0.75
	Anisotropic local	**98.30**	98.29 ± 2.65	**88.69**	**91.52 ± 10.42**	**3.62**	**2.72 ± 1.76**	**1.69**	**1.49 ± 0.75**
	Isotropic	97.80	98.12 ± 1.60	81.45	85.23 ± 11.34	16.12	11.29 ± 5.43	2.17	1.88 ± 0.59
	ICOV	97.95	98.25 ± 1.34	80.89	84.50 ± 10.29	17.36	13.11 ± 5.22	2.09	1.90 ± 0.56
NW-MA	Anisotropic	98.29	**98.64 ± 1.72**	82.32	87.13 ± 13.44	6.85	4.33 ± 3.26	1.82	1.54 ± 0.71
	Anisotropic local	**98.39**	98.33 ± 2.72	**87.27**	**90.12 ± 12.66**	**3.29**	**2.79 ± 1.83**	**1.60**	**1.48 ± 0.72**
	Isotropic	97.60	97.74 ± 2.00	78.70	82.12 ± 13.09	17.71	13.39 ± 6.17	2.12	1.95 ± 0.59
	ICOV	97.79	97.96 ± 1.64	79.20	82.05 ± 12.28	19.32	14.79 ± 5.70	2.12	1.96 ± 0.56
FW-LI	Anisotropic	95.00	96.26 ± 3.21	59.21	67.79 ± 18.40	20.63	9.80 ± 4.35	2.60	2.13 ± 0.64
	Anisotropic local	95.79	96.71 ± 4.43	**77.23**	**82.55 ± 16.93**	**5.13**	**3.53 ± 2.29**	**1.58**	**1.43 ± 0.83**
	Isotropic	**96.71**	96.70 ± 3.42	67.76	72.67 ± 16.50	22.38	12.59 ± 6.64	2.29	1.96 ± 0.63
	ICOV	96.60	**96.81 ± 3.16**	66.75	71.74 ± 16.43	25.16	14.41 ± 6.74	2.41	2.08 ± 0.61
NW-LI	Anisotropic	94.67	95.81 ± 3.82	57.09	64.49 ± 19.24	20.12	11.20 ± 4.61	2.73	2.31 ± 0.52
	Anisotropic local	**96.37**	**96.70 ± 5.70**	**75.15**	**82.73 ± 18.12**	**6.43**	**3.78 ± 2.49**	**1.81**	**1.55 ± 0.86**
	Isotropic	96.06	96.00 ± 3.61	63.80	69.28 ± 15.79	28.37	16.78 ± 7.53	2.54	2.26 ± 0.56
	ICOV	95.94	96.14 ± 3.18	62.96	68.07 ± 15.63	30.02	18.33 ± 7.40	2.64	2.38 ± 0.51

respect to the ICOV and Gaussian derivative-based methods. It is also observed, however, that the other anisotropic approach provides much lower *AUC-PR*. The comparison between the MA and LI graphs allows to evaluate the actual contribution of the proposed local orientation estimation for the combination of filters and non-maximum suppression. Note that the MA contours are more continuous, more linear, and of higher contrast, while the LI contours are much harder to detect because of the lower contrast and the more complex shape. For this reason, it is more probable that the star shape artifacts, removed by the local orientation approach, affect the LI detection to a higher degree.

The resulting PR curves for tolerance $\tau = 3\ px$ are depicted in Fig. 5, along with the evolution of the corresponding number of connected components (CC/PP), and the average distance to TP ($d(TP)$), with varying recall. Upon the evaluation of these statistics, it is observed that the isotropic and the ICOV approaches provide similar results. The anisotropic approaches achieve higher precision at higher recall for the MA contours, and the proposed method provides the best results regardless of the evaluated contour. The quality of the detected contours using the proposed method is significantly higher than using the other approaches. It is remarkable that the ratio of connected components remains almost constant regardless of the recall and the analysed contours, and much lower than other methods. Also the achieved location error is much lower, with almost $1/2\ px$ difference with the reference methods.

Table 1 provides a summary of the analysed statistics at 90% recall. In this case, results for the global and the image-wise approaches for statistic computation are provided, along with ROC curve AUC results. The *AUC-ROC* values are much higher and overlapped than the *AUC-PR* results, showing no clear preference for any detection method. The *AUC-PR* shows the clear advantages of the proposed method against the compared alternatives. In addition, it is also observed that not only a global threshold provides better results with the proposed method, but there is also more room for improvement if the optimal threshold is selected for each image, in comparison with the other methods, as evidenced by the better image-wise values.

4. Conclusions

We present a new method for the robust detection of carotid artery layer contours in B-mode ultrasound images based on anisotropic filters and local orientation estimation. The use of anisotropic Gaussian derivative filters is motivated by the need of advanced cues to differentiate real edges from noise edges in ultrasound images. Traditional denoising cues based on speckle noise parameter estimation from constant regions do not seem suitable for the artery

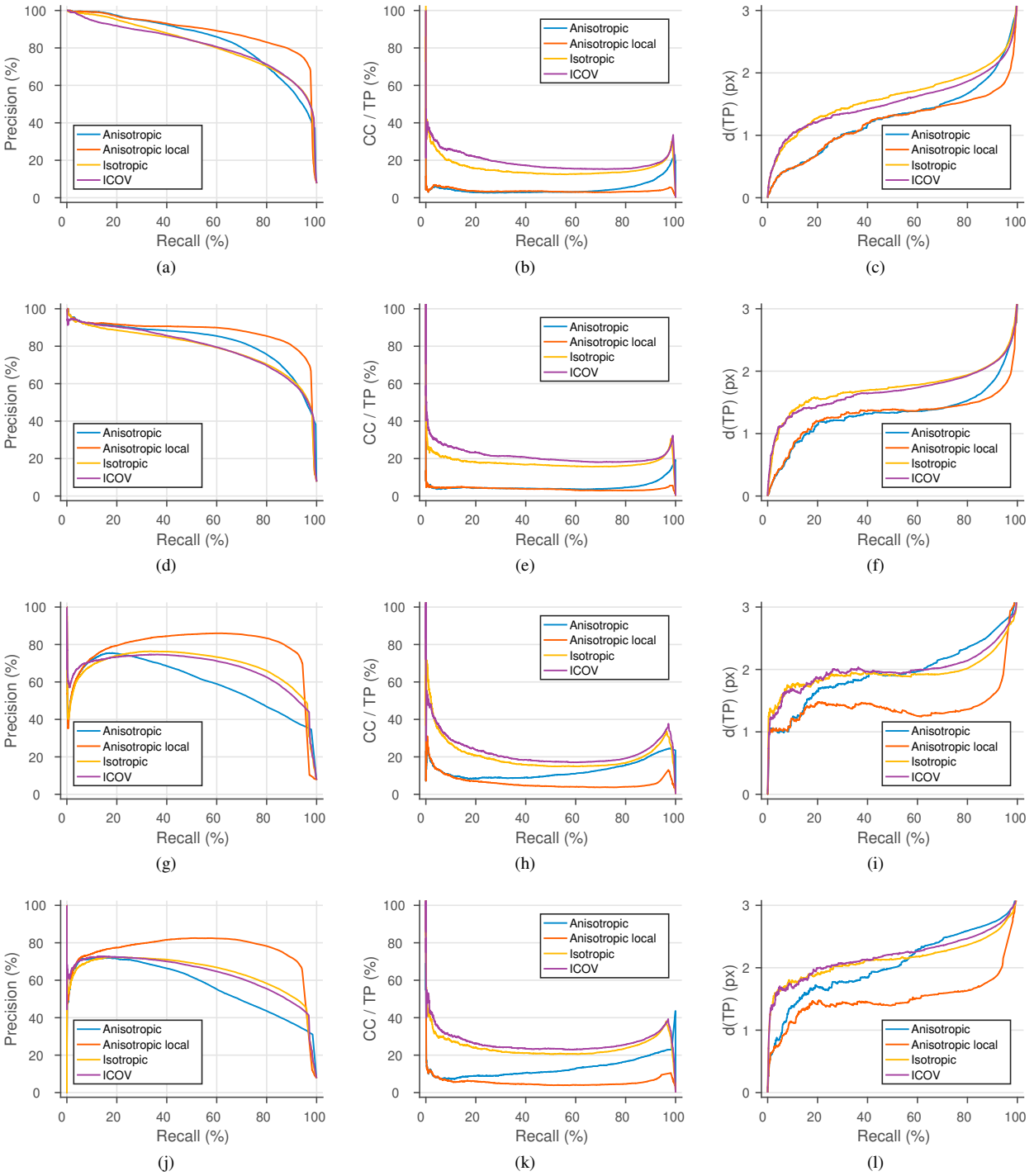

Fig. 5: Comparison results measured for tolerance $\tau = 3$ with respect to recall. Precision-recall curves (a,d,g,j), percentage of connected components per true positive for varying recall (b,e,h,k), and average distance between the true positives and the ground truth for varying recall (c,f,i,l), for the different target contours. (a-c) Far-wall media-adventitia. (d-f) Near-wall media-adventitia. (g-i) Far-wall lumen-intima. (j-l) Near-wall lumen-intima. The results show that the proposed anisotropic edge detector, using the non-maximum suppression over local orientation, allows to detect higher quality contours with higher precision, regardless of the required recall rate and the evaluated intima-media contour.

layer regions, where the regions are too narrow. Instead, the anisotropic filters allow using a wider integration scale along the edge direction, enhancing low contrast coherent edges following low curvature contours, while preserving the edge location precision. However, this approach also generates false edges near both isolated and high curvature contours. The effect of these false edges is reduced using the proposed local orientation estimation approach, by enforcing the existence of few strong orientations on each image location. This allows a robust and precise method for edge detection in carotid ultrasound images, as it is demonstrated by the presented results. Future work involves optimal threshold selection methods for each image and the integration of the proposed methods on carotid intima-media segmentation algorithms.

5. Acknowledgments

This work is funded by the North Portugal Regional Operational Programme (NORTE 2020), under the PORTUGAL 2020 Partnership Agreement, and the European Regional Development Fund (ERDF), within the project "NanoSTIMA: Macro-to-Nano Human Sensing: Towards Integrated Multimodal Health Monitoring and Analytics/NORTE-01-0145-FEDER-000016".

References

1. Davis, N.. Atherosclerosis - An Inflammatory Process. *Journal of Medical Insurance* 2005;**37**:72–75.
2. Touboul, P.J., et al., . Mannheim Carotid Intima-Media Thickness Consensus (2004-2006-2011). An Update on Behalf of the Advisory Board of the 3rd, 4th and 5th Watching the Risk Symposium 13th, 15th and 20th European Stroke Conferences, Mannheim, Germany, 2004, Brussels, Belgium, 2006 and Hamburg, Germany, 2011. *Cerebrovasc Dis* 2012;**34**:290–296.
3. Stein, J.H., Hennerici, M.G., Meairs, S., et al., . Use of carotid ultrasound to indentify subclinical vascular disease and evaluate cardiovascular disease risk: a consensus statement from the American Society of Echocardiography Carotid Intima-Media Thickness Task Force endorsed by the Society for Vascular Medicine. *J Am Soc Echocardiog* 2008;**21**:93–111.
4. Amato, M., Montorsi, P., Ravani, A., et al., . Carotid intima-media thickness by B-mode ultrasound as surrogate of coronary atherosclerosis: correlation with quantitative coronary angiography and coronary intravascular ultrasound findings. *Eur Heart J* 2007;**28**:2094–2101.
5. Baldassarre, D., Amato, M., Pustina, L., et al., . Measurement of carotid artery intima-media thickness in dyslipidemic patients increases the power of traditional risk factors to predict cardiovascular events. *Atherosclerosis* 2007;**191**:403–408.
6. Lorenz, M.W., Markus, H.S., Bots, M.L, et al., . Prediction of clinical cardiovascular events with carotid intima-media thickness: a systematic review and meta-analysis. *Circulation* 2007;**115**:459–467.
7. Nambi, V., Chambless, L., He M., et al., . Common carotid artery IMT is as good as carotid IMT of all carotid artery segments in improving prediction of coronary heart disease risk in the Atherosclerosis Risk in Communities (ARIC) study. *Eur Heart J* 2012;**33**:183–190.
8. Loizou, C.. A review of ultrasound common carotid image and video segmentation techniques. *Med Biol Eng Comput* 2014;**52**(12):1073–93.
9. Molinari, F., Zeng, G., Suri, J.. A state of the art review on intima-media thickness (IMT) measurement and wall segmentation techniques for carotid ultrasound. *Comput Meth Prog Bio* 2010;**100**(3):201–221.
10. Xu, X., Zhou, Y., Cheng, X., Song, E., Li, G.. Ultrasound intima-media segmentation using Hough transform and dual snake model. *Comp Med Imag Graph* 2012;**36**:248–258.
11. Zhou, Y., Cheng, Y., Xu, X., E., S.. Dynamic programming in parallel boundary detection with application to ultrasound intima-media segmentation. *Med Image Anal* 2013;**17**:892–906.
12. Loizou, C., Pattichis, C., Pantziaris, M., Nicolaides, A.. An integrated system for the segmentation of atherosclerotic carotid plaque. *IEEE T Inf Technol B* 2007;**11**(6):661–667.
13. Loizou, C., Petroudi, S., Pantziaris, M., Nicolaides, A., Pattichis, C.. An Integrated System for the Segmentation of Atherosclerotic Carotid Plaque Ultrasound Video. *IEEE T Ultrason Ferr* 2014;**61**(1):86–101.
14. Destrempes, F., Meunier, J., Giroux, M.F., Soulez, G., Cloutier, G.. Segmentation of Plaques in Sequences of Ultrasonic B-Mode Images of Carotid Arteries Based on Motion Estimation and a Bayesian Model. *IEEE T Bio-med Eng* 2011;**58**(8):2202–2211.
15. Rocha, R., Campilho, A., Silva, J., Azevedo, E., Santos, R.. Segmentation of the carotid intima-media region in B-mode ultrasound images. *Image Vision Comput* 2010;**28**:614–625.
16. Rocha, R., Silva, J., Campilho, A.. Automatic segmentation of carotid B-mode images using fuzzy classification. *Med Biol Eng Comput* 2012;**50**:533–545.
17. Rouco, J., Campilho, A.. Robust Common Carotid Artery Lumen Detection in B-Mode Ultrasound Images using Local Phase Symmetry. In: *Int Conf Acoust Spee (ICASSP), 2013*. 2013, p. 929–933.
18. Rouco, J., Azevedo, E., Campilho, A.. Automatic Lumen Detection on Longitudinal Ultrasound B-Mode Images of the Carotid Using Phase Symmetry. *Sensors* 2015;**16**(3):350.
19. Yu, Y., Acton, S.. Edge detection in ultrasound imagery using the instantaneus coefficient of variation. *IEEE T Image Process* 2004;**13**(12):1640–55.
20. Yu, Y., Acton, S.. Speckle reduced anisotropic diffusion. *IEEE T Image Process* 2002;**11**(11):1269–1270.
21. Geusebroek, J., Smeulders, A., van de Weijer, J.. Fast anisotropic Gauss filtering. *IEEE T Image Process* 2003;**12**(8):938–943.
22. Bowyer, K., Kranenburg, C., Dougherty, S.. Edge Detector Evaluation Using Empirical ROC Curves. *Comp Vis Imag Und* 2001;**84**:77–103.